Possible existence of chiral and multiple chiral nuclei in thallium isotopes*

Rui-Ju Guo(郭睿巨) Xiao Lu(陆晓) Bin Qi(亓斌)† Chen Liu(刘晨)‡ Shou-Yu Wang(王守宇)

Shandong Provincial Key Laboratory of Optical Astronomy and Solar-Terrestrial Environment, Institute of Space Sciences, Shandong University, Weihai 264209, China

Abstract: The chirality in thallium isotopes is investigated using the adiabatic and configuration-fixed constrained triaxial relativistic mean field theory. Several minima with prominent triaxial deformation and proper configuration, where the chiral doublet bands may appear, are obtained in odd-odd nuclei ^{192,194,196,198}Tl and odd-mass nuclei ^{193,195,197}Tl. Furthermore, the possible existence of multiple chiral doublet bands (MχD) is demonstrated in ^{192,193,194,195,196,197,198}Tl. As the chiral doublet bands in ^{193,194,198}Tl and MχD in ^{195}Tl have been observed experimentally, further experimental exploration for the chirality in ^{192,196,197}Tl and MχD in thallium isotopes is expected to verify the predictions.

Keywords: chirality, relativistic mean field theory, thallium isotopes

DOI: 10.1088/1674-1137/ac6248

I. INTRODUCTION

Chirality is a subject of general interest in physics, chemistry, and biology. Chirality in atomic nuclei was predicted in 1997 [1], which has been a prominent topic for the past two decades. In the rotating triaxial nucleus with the unpaired particle(s) and hole(s) in the high-j orbital, the particle(s) and hole(s) align their angular momentum vectors along the short and long axes, respectively, while the collective rotation vector of the core aligns along the intermediate axis, which can form a chiral system. Due to quantum tunneling, a pair of nearly degenerate $\Delta I = 1$ bands with the same parity, i.e., chiral doublet bands, can be observed experimentally [1]. Since the chiral doublet bands were first observed experimentally [2], more than 50 candidates have been reported in the $A\sim$ 80,100,130, and 190 [3–11] mass regions. In 2006, Meng *et al.* [12] suggested that more than one pair of chiral doublet bands can exist in one single nucleus, which are called multiple chiral doublet (MχD) bands. To date, experimental evidence for the MχD bands has been observed in ^{78}Br [13], ^{81}Kr [9], ^{103}Rh [14], ^{105}Rh [15, 16], ^{107}Ag [17–19], ^{133}Ce [20], ^{135}Nd [21, 22], ^{136}Nd [23], and ^{195}Tl [24]. Theoretically, since the chiral symmetry breaking was first predicted using the tilted axis cranking (TAC) approach and particle-rotor model (PRM) [1], numerous efforts have been devoted toward the development of the TAC [25–29] and PRM methods [25, 26, 30–50] to describe chiral rotation in atomic nuclei. Meanwhile, the interacting boson-fermion model approach [51, 52], collective Hamiltonian method [53, 54], angular momentum projection method [55, 56], random phase approximation [57], and critical point symmetries method [58] have also been developed to study chiral doublet bands and have yielded considerable success. An overview of these studies and open problems for understanding the nuclear chirality are introduced in Refs. [3–5, 7].

So far, many candidate chiral nuclei have been reported in the 80,100, and 130 mass regions [6, 7], forming three "islands of chiral nuclei". In comparison, only five candidate chiral nuclei have been reported in the 190 mass region, namely, ^{193,194,195,198}Tl [24, 59–65] and ^{188}Ir [66]. In 2008, candidate chiral doublet bands with the $\pi h^1_{9/2}\otimes\nu i^{-1}_{13/2}$ configuration were observed in ^{198}Tl [64]. The two-quasiparticle-plus-triaxial-rotor model calculations suggested an aplanar orientation of the total angular momenta for these bands, thus supporting possible chirality [64, 65]. From 2011 to 2014, a pair of rotational bands associated with the $\pi h^1_{9/2}\otimes\nu i^{-1}_{13/2}$ configuration at lower spins and the $\pi h^1_{9/2}\otimes\nu i^{-3}_{13/2}$ configuration at higher spins were reported in ^{194}Tl [61–63]. These bands were suggested as chiral geometry in the angular momentum space owing to their near-degeneracy in the excitation energies

Received 7 January 2022; Accepted 30 March 2022; Published online 8 June 2022

* This work is partly support by the Major Program of Natural Science Foundation of Shandong Province (ZR2020ZD30), the Outstanding Youth Fund of Natural Science Foundation of Shandong Province (ZR2020YQ07), the National Natural Science Foundation of China (11675094, 12075138), and the Young Scholars Program of Shandong University, Weihai. The computations were carried out on the supercomputing system in the Supercomputing Center and an HP Proliant DL785G6 server hosted by the Institute of Space Science in Shandong University, Weihai

† E-mail: bqi@sdu.edu.cn

‡ E-mail: cliu@sdu.edu.cn

and similar alignments and $B(M1)/B(E2)$ reduced transition probability ratios [61–63]. The chirality in ^{194}Tl was also supported by the two-quasiparticle-plus-triaxial-rotor model and Cranked Nilsson Strutinsky model [61–63].

In 2017, three negative-parity bands based on the $\pi h^{1}_{9/2}\otimes\nu i^{-2}_{13/2}$ configurations with close excitation energies and almost equal $B(M1)/B(E2)$ values were identified in ^{193}Tl, which suggested that one or two chiral systems were formed [59]. Theoretical calculations with the Cranked Nilsson Strutinsky model suggested the triaxial shape of ^{193}Tl and thus supported the presence of chirality [59, 60]. In 2018, two pairs of nearly degenerate bands based on the $\pi h^{1}_{9/2}\otimes\nu i^{-2}_{13/2}$ and $\pi i^{1}_{13/2}\otimes\nu(fp)^{1}i^{-3}_{13/2}$ configurations were identified in ^{195}Tl [24], which signified the first evidence of MχD in the 190 mass region. The Total Routhian surface (TRS) and relativistic mean field (RMF) calculations predicted triaxial shapes for both configurations [24, 50].

It is naturally interesting to search for and predict the chirality or MχD phenomenon of thallium isotopes in the $A\sim 190$ mass region. The triaxial deformation and suitable unpaired high-j particles-holes configurations are necessary for the prediction of the candidate chiral nuclei, which can be obtained from the fully microscopic self-consistent RMF theory [67]. The RMF has obtained great success in predicting and describing interesting physics [68– 79]. Thus, we adopt the constrained triaxial RMF theory to search for the candidate nuclei of chirality and MχD in thallium isotopes.

II. FORMALISM AND NUMERICAL DETAIL

The starting point of the RMF theory is the standard effective Lagrangian density constructed with the degrees of freedom associated with a nucleon field (ψ), two isoscalar meson fields (σ and ω_μ), the isovector meson field ($\vec{\rho}_\mu$), and the photon field (A_μ). This theory has been successfully applied to study triaxial shape coexistence and possible MχD in many nuclei, e.g., Co isotopes [80], As isotopes [81], Br isotopes [82], Rb isotopes [83], ^{104,106,108,110}Rh [84, 85], ^{103,105}Rh [86, 14], ^{107}Ag [87], ^{125,129,131}Cs [88], ^{133}Ce [20], and ^{195}Tl [50]. Here, only a brief introduction to the triaxial RMF is provided; a detailed formalism can be found in Ref. [12]. Under the "mean-field" and "no-sea" approximations, one can derive the corresponding energy-density functional, from which one can obtain the equation of motion for a single-nucleon orbit $\psi_i(\boldsymbol{r})$ with the help of the variational principle

$$\{\alpha\cdot[\boldsymbol{p}-\boldsymbol{V}(\boldsymbol{r})]+\beta m^{*}(\boldsymbol{r})+V_0(\boldsymbol{r})\}\psi_i(\boldsymbol{r})=\epsilon_i\psi_i(\boldsymbol{r}). \quad (1)$$

Here, $m^{*}(\boldsymbol{r})$ is defined as $m^{*}(\boldsymbol{r})\equiv m+g_\sigma\sigma(\boldsymbol{r})$, with m referring to the mass of the bare nucleon. The repulsive-vector potential $V_0(\boldsymbol{r})$, i.e., the time-like component of the vector potential is given by

$$V_0(\boldsymbol{r})=g_\omega\omega_0(\boldsymbol{r})+g_\rho\tau_3\rho_0(\boldsymbol{r})+e\frac{1-\tau_3}{2}A_0(\boldsymbol{r}), \quad (2)$$

where $g_\sigma, g_\omega, g_\rho$ are the coupling strengths between the nucleons and mesons, and $\tau_3=1$ (-1) for neutrons (protons). The time-odd fields $\boldsymbol{V}(\boldsymbol{r})$ are given by the space-like components of the vector fields

$$\boldsymbol{V}(\boldsymbol{r})=g_\omega\boldsymbol{\omega}(\boldsymbol{r})+g_\rho\tau_3\boldsymbol{\rho}(\boldsymbol{r})+e\frac{1-\tau_3}{2}\boldsymbol{A}(\boldsymbol{r}). \quad (3)$$

Each Dirac spinor $\psi_i(\boldsymbol{r})$ is expanded in terms of a set of three-dimensional harmonic-oscillator (HO) bases in Cartesian coordinates with 12 major shells. The meson fields that provide the nuclear mean-field potentials are expanded in terms of the same HO basis as these Dirac spinors but with 20 major shells. Due to the Pauli block effect, pairing correlations are neglected.

The calculated results with the parameter set PK1 [89] are shown in this paper, and it has been verified that a very similar conclusion can be obtained adopting the NL3 [90], PC-PK1 [78] parameter sets. We use constrained calculation with $\langle\hat{Q}^2_{20}+2\hat{Q}^2_{22}\rangle$, i.e., β^2_2, to find the ground state of triaxial deformed nuclei. In the process of the β-constrained calculation, triaxial deformation is automatically obtained by minimizing the energy. During the calculation, different configurations can be obtained by adiabatic constrained calculation, and then, the configuration-fixed constrained calculation is performed. Here, the adiabatic constrained calculation indicates that the nucleon always occupies the lowest single-particle levels, while the configuration-fixed constrained calculation suggests that the nucleon must occupy the same combination of the single-particle levels during the constraint process [12, 84].

III. RESULTS AND DISCUSSION

The calculated potential-energy curves for the odd-odd nuclei ^{192,194,196,198,200}Tl, based on the adiabatic and configuration-fixed constrained triaxial RMF theory, are presented in the upper panel of Fig. 1, while the results for the odd-mass nuclei ^{193,195,197,199}Tl are presented in the upper panel of Fig. 2. The minima in the potential-energy curves for the fixed configurations are represented by stars and labeled as A to J. The triaxiality parameter γ obtained by minimizing the energy is given as a function of β in the lower panel of Fig. 1 and Fig. 2. The shaded areas in the figures represent the triaxiality parameter γ favorable for nuclear chirality. In our calculations, the quadrupole deformation parameter β is constrained from

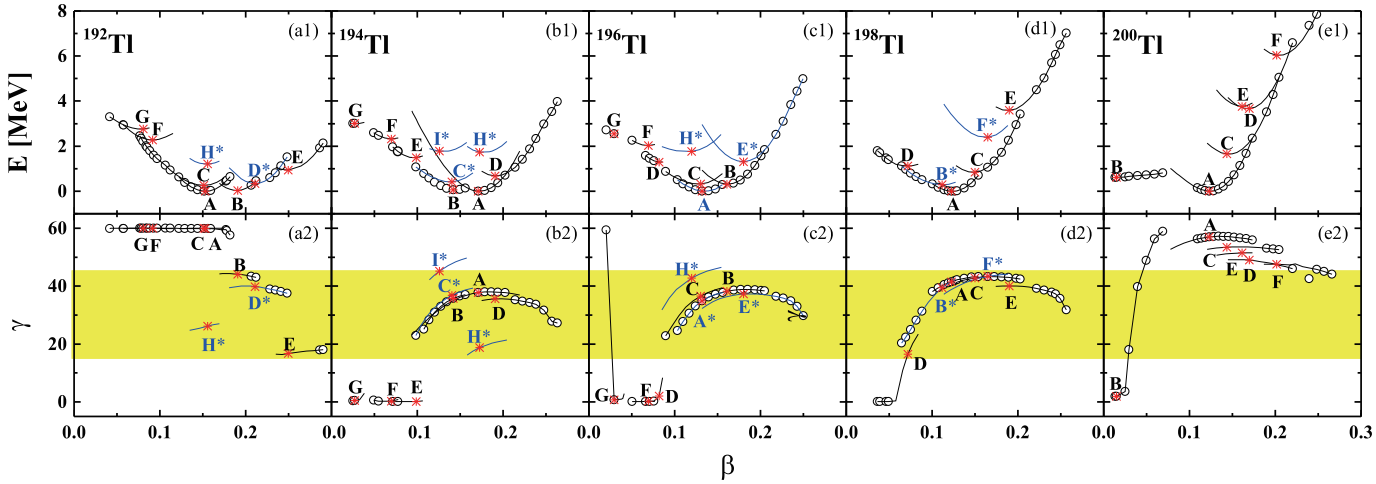

Fig. 1. (color online) The calculated potential-energy curves E (in MeV) and triaxiality parameter γ (in degrees) as functions of the deformation parameter β for the odd-odd nuclei ^{192,194,196,198,200}Tl. The open circles and solid lines represent the results for the adiabatic and configuration-fixed constrained triaxial RMF calculations with the PK1 parameter set. The minima in the energy curves for the fixed configuration are represented by stars and labeled as A, B, C, D, E, F, G, and H, respectively. The suitable states for the appearance of chirality are marked in blue with asterisks. The shaded area represents the triaxiality parameter γ, favorable for nuclear chirality.

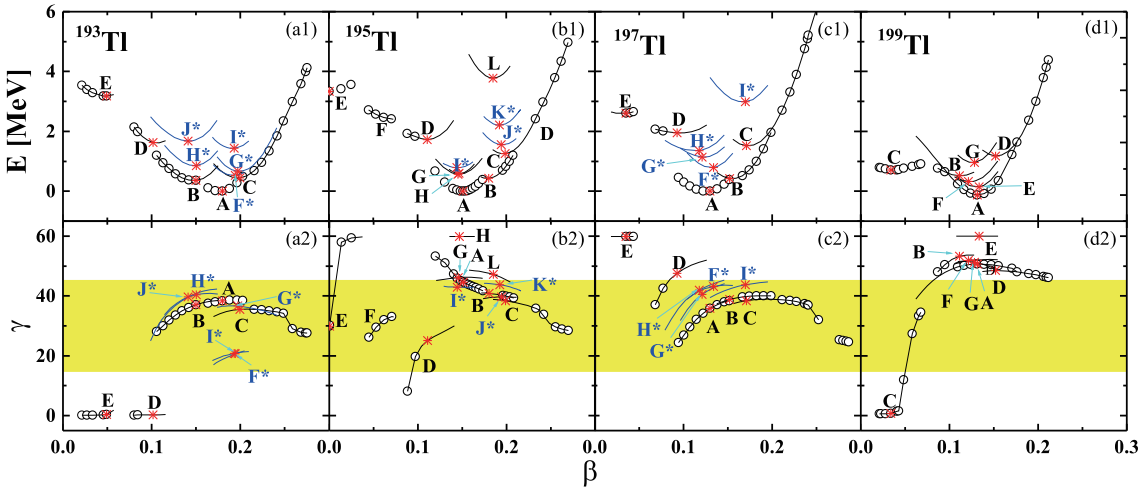

Fig. 2. (color online) Same as Fig. 1, but for the odd-mass nuclei ^{193,195,197,199}Tl.

0 to 0.5. As there are no suitable chiral configurations for $\beta > 0.3$, only the results of $\beta < 0.3$ are exhibited here.

As triaxial deformation is the necessary condition for nuclear chirality, we first search for the minima with prominent triaxial deformation. As shown in Fig. 1 and Fig. 2, more than one triaxial local minimum is found in ^{192,193,194,195,196,197,198}Tl, which provide good examples of triaxial shape coexistence. As the neutron number increases, the quadrupole deformation parameter of the ground states in the Tl isotopes decreases, and the energy of the excited states increases. For ^{199}Tl, the calculations show that there is no suitable triaxial minimum, although the 3-quasiparticle band based on the $\pi h^{1}_{9/2}\otimes\nu i^{-2}_{13/2}$ configuration has been observed experimentally [91]. For ^{200}Tl, the oblate band based on the high-j particle hole configuration $\pi h^{1}_{9/2}\otimes\nu i^{-1}_{13/2}$ has been extended beyond the particle alignment frequencies [92], and our results also show that there is no suitable triaxial deformation in these nuclei. Therefore, ^{199,200}Tl can be ruled out from the suggested candidate chiral nuclei.

Apart from triaxial deformation, the proper particles-holes configuration is also necessary for the appearance of the chiral doublet bands. By performing the configuration-fixed constrained calculations, the single-particle levels for a certain configuration can be obtained as functions of the deformation β [12]. Considering the ground state and excited states with particle-hole configurations of ^{194}Tl and ^{199}Tl as examples, the proton and neutron single-particle levels obtained are presented in Fig. 3. The positive (negative) parity states are marked by solid

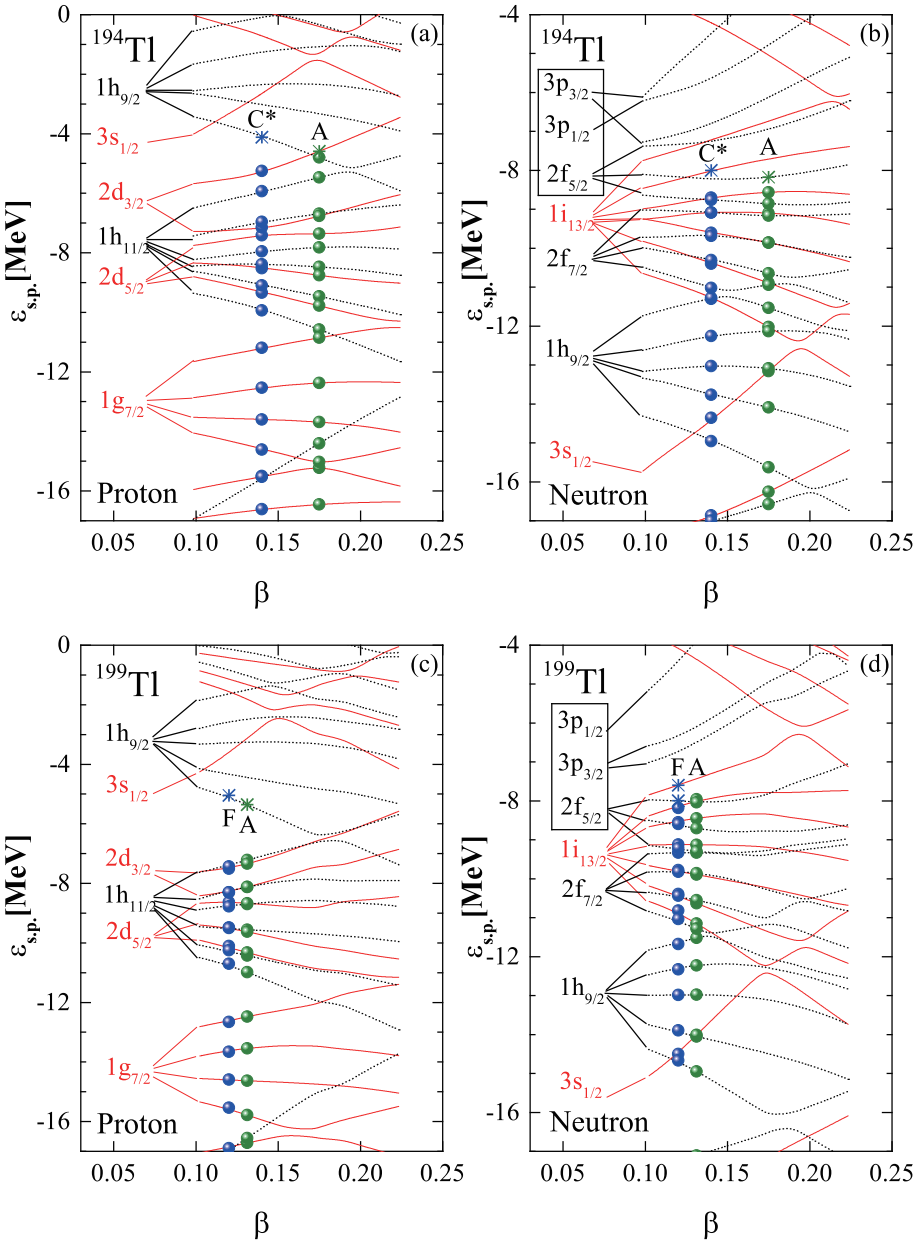

Fig. 3. (color online) Proton and neutron single-particle levels obtained for constrained triaxial RMF calculations as functions of the deformation β for the ground state and excited states with particle-hole configurations of ^{194}Tl (upper panel) and ^{199}Tl (lower panel). The positive (negative) parity states are marked by solid (dot) lines and the occupations of the ground states (olive) and excited states (blue) are represented by filled circles (two particles) and stars (one particle).

(dashed) lines and the occupations of the ground states are represented by filled circles (two particles) and stars (one particle). The corresponding quantum numbers for the spherical case are labeled on the left side of the levels.

The calculated total energies $E_{\rm tot}$, excited energies relative to the ground state E_x(cal.), triaxial deformation parameters β and γ, corresponding valence nucleon, and unpaired nucleon configurations of the minima are given in Tables 1 and 2. The valence proton configurations take reference of 82 nucleons, which occupy the states below the 82 major-shell. The valence neutron configurations take reference of 114 nucleons, which occupy the states below the 126 major-shell except for the $3p_{3/2}$, $3p_{1/2}$, and $2f_{5/2}$ subshells. As it is difficult to distinguish the occupation in the low-j orbits $3p_{3/2}$, $3p_{1/2}$, and $2f_{5/2}$, we denote the nucleons in the three subshells as $(fp)^n$ in the tables. As the nuclear chirality of thallium isotopes is essentially determined by the high-j $1i_{13/2}$ and $1h_{9/2}$, such illegibility does not influence the conclusions drawn here. Combining the calculated deformations and configurations, we find the suitable states for the appearance of chirality, which are marked in blue with asterisks in the

Table 1. The total energies $E_{\rm tot}$, excited energies relative to the ground state E_x(cal.), triaxial deformation parameters β and γ, and their corresponding valence nucleon configurations of minima for states in the configuration-fixed constrained triaxial RMF calculations for the odd-odd nuclei $^{192-200}$Tl. The configurations of the valence proton take reference of 82 nucleons, and those of the valence neutron take reference of 114 nucleons. The suitable states for the appearance of chirality are marked in blue with asterisks.

Nuclei	States	Configuration		$E_{\rm tot}$ /MeV	(β,γ)	E_x(cal.) /MeV
		Valence nucleons	Unpaired nucleons			
^{192}Tl	A	$\pi(s_{1/2}^{-2}h_{9/2}^{1})\otimes\nu[(fp)^3i_{13/2}^{-6}]$	$\pi h_{9/2}^{1}\otimes\nu(fp)^1$	−1506.26	(0.15,59.82°)	0
	B	$\pi(d_{3/2}^{-1}s_{1/2}^{-2}h_{9/2}^{2})\otimes\nu[(fp)^2i_{13/2}^{-5}]$	$\pi d_{3/2}^{-1}\otimes\nu i_{13/2}^{-1}$	−1506.23	(0.19,44.15°)	0.03
	C	$\pi(s_{1/2}^{-2}h_{9/2}^{1})\otimes\nu[(fp)^2i_{13/2}^{-5}]$	$\pi h_{9/2}^{1}\otimes\nu i_{13/2}^{-1}$	−1506.00	(0.15,59.94°)	0.26
	D*	$\pi(d_{3/2}^{-2}s_{1/2}^{-2}h_{9/2}^{3})\otimes\nu[(fp)^2i_{13/2}^{-5}]$	$\pi h_{9/2}^{1}\otimes\nu i_{13/2}^{-1}$	−1505.92	(0.21,39.84°)	0.34
	E	$\pi(d_{3/2}^{-2}s_{1/2}^{-2}h_{11/2}^{-2}h_{9/2}^{5})\otimes\nu[f_{7/2}^{-2}(fp)^3i_{13/2}^{-4}]$	$\pi h_{9/2}^{1}\otimes\nu(fp)^1$	−1505.32	(0.25,16.72°)	0.94
	F	$\pi(s_{1/2}^{-1})\otimes\nu[(fp)^2i_{13/2}^{-5}]$	$\pi s_{1/2}^{-1}\otimes\nu i_{13/2}^{-1}$	−1503.99	(0.09,59.93°)	2.27
	G	$\pi(s_{1/2}^{-1})\otimes\nu[(fp)^1i_{13/2}^{-4}]$	$\pi s_{1/2}^{-1}\otimes\nu(fp)^1$	−1503.50	(0.08,59.94°)	2.76
	H*	$\pi(s_{1/2}^{-2}h_{9/2}^{1})\otimes\nu[f_{7/2}^{-2}(fp)^2i_{13/2}^{-3}]$	$\pi h_{9/2}^{1}\otimes\nu i_{13/2}^{-1}$	−1505.06	(0.16,26.17°)	1.20
^{194}Tl	A	$\pi(d_{3/2}^{-1}s_{1/2}^{-2}h_{9/2}^{2})\otimes\nu[(fp)^3i_{13/2}^{-4}]$	$\pi d_{3/2}^{-1}\otimes\nu(fp)^1$	−1523.19	(0.17,37.74°)	0
	B	$\pi(s_{1/2}^{-2}h_{9/2}^{1})\otimes\nu[(fp)^3i_{13/2}^{-4}]$	$\pi h_{9/2}^{1}\otimes\nu(fp)^1$	−1523.12	(0.14,35.68°)	0.07
	C*	$\pi(s_{1/2}^{-2}h_{9/2}^{1})\otimes\nu[(fp)^2i_{13/2}^{-3}]$	$\pi h_{9/2}^{1}\otimes\nu i_{13/2}^{-1}$	−1522.77	(0.14,36.81°)	0.42
	D	$\pi(d_{3/2}^{-2}s_{1/2}^{-2}h_{9/2}^{3})\otimes\nu[(fp)^3i_{13/2}^{-4}]$	$\pi h_{9/2}^{1}\otimes\nu(fp)^1$	−1522.51	(0.19,35.61°)	0.68
	E	$\pi(s_{1/2}^{-1})\otimes\nu[(fp)^2i_{13/2}^{-3}]$	$\pi s_{1/2}^{-1}\otimes\nu i_{13/2}^{-1}$	−1521.79	(0.10,0.19°)	1.49
	F	$\pi(s_{1/2}^{-1})\otimes\nu[(fp)^1i_{13/2}^{-2}]$	$\pi s_{1/2}^{-1}\otimes\nu(fp)^1$	−1520.86	(0.07,0.27°)	2.33
	G	$\pi(s_{1/2}^{-1})\otimes\nu[i_{13/2}^{-1}]$	$\pi s_{1/2}^{-1}\otimes\nu i_{13/2}^{-1}$	−1520.19	(0.03,0.47°)	3.00
	H*	$\pi(d_{3/2}^{-2}s_{1/2}^{-2}h_{9/2}^{3})\otimes\nu[(fp)^2i_{13/2}^{-3}]$	$\pi h_{9/2}^{1}\otimes\nu i_{13/2}^{-1}$	−1521.46	(0.17,18.80°)	1.73
	I*	$\pi(s_{1/2}^{-2}h_{9/2}^{1})\otimes\nu[(fp)^2i_{13/2}^{-3}]$	$\pi h_{9/2}^{1}\otimes\nu i_{13/2}^{-1}i_{13/2}^{-1}i_{13/2}^{-1}$	−1521.42	(0.13,45.19°)	1.78
^{196}Tl	A*	$\pi(s_{1/2}^{-2}h_{9/2}^{1})\otimes\nu[(fp)^4i_{13/2}^{-3}]$	$\pi h_{9/2}^{1}\otimes\nu i_{13/2}^{-1}$	−1539.43	(0.13,34.88°)	0
	B	$\pi(d_{3/2}^{-1}s_{1/2}^{-2}h_{9/2}^{2})\otimes\nu[(fp)^4i_{13/2}^{-3}]$	$\pi d_{3/2}^{-1}\otimes\nu i_{13/2}^{-1}$	−1539.12	(0.16,38.25°)	0.31
	C	$\pi(s_{1/2}^{-2}h_{9/2}^{1})\otimes\nu[(fp)^3i_{13/2}^{-2}]$	$\pi h_{9/2}^{1}\otimes\nu(fp)^1$	−1539.11	(0.13,36.56°)	0.32
	D	$\pi(s_{1/2}^{-1})\otimes\nu[(fp)^3i_{13/2}^{-2}]$	$\pi s_{1/2}^{-1}\otimes\nu(fp)^1$	−1538.15	(0.08,2.10°)	1.28
	E*	$\pi(d_{3/2}^{-2}s_{1/2}^{-2}h_{9/2}^{3})\otimes\nu[(fp)^4i_{13/2}^{-3}]$	$\pi h_{9/2}^{1}\otimes\nu i_{13/2}^{-1}$	−1538.12	(0.18,37.26°)	1.31
	F	$\pi(s_{1/2}^{-1})\otimes\nu[(fp)^2i_{13/2}^{-1}]$	$\pi s_{1/2}^{-1}\otimes\nu i_{13/2}^{-1}$	−1537.40	(0.07,0.21°)	2.03
	G	$\pi(s_{1/2}^{-1})\otimes\nu[(fp)^1]$	$\pi s_{1/2}^{-1}\otimes\nu(fp)^1$	−1536.88	(0.03,0.77°)	2.55
	H*	$\pi(s_{1/2}^{-2}h_{9/2}^{1})\otimes\nu[(fp)^2i_{13/2}^{-1}]$	$\pi h_{9/2}^{1}\otimes\nu i_{13/2}^{-1}$	−1,537.67	(0.12,42.75°)	1.77
^{198}Tl	A	$\pi(s_{1/2}^{-2}h_{9/2}^{1})\otimes\nu[(fp)^5i_{13/2}^{-2}]$	$\pi h_{9/2}^{1}\otimes\nu(fp)^1$	−1555.14	(0.12,41.49°)	0
	B*	$\pi(s_{1/2}^{-2}h_{9/2}^{1})\otimes\nu[(fp)^4i_{13/2}^{-1}]$	$\pi h_{9/2}^{1}\otimes\nu i_{13/2}^{-1}$	−1554.86	(0.11,39.43°)	0.28
	C	$\pi(d_{3/2}^{-1}s_{1/2}^{-2}h_{9/2}^{2})\otimes\nu[(fp)^5i_{13/2}^{-2}]$	$\pi d_{3/2}^{-1}\otimes\nu(fp)^1$	−1554.30	(0.15,42.84°)	0.84
	D	$\pi(s_{1/2}^{-1})\otimes\nu[(fp)^4i_{13/2}^{-1}]$	$\pi s_{1/2}^{-1}\otimes\nu i_{13/2}^{-1}$	−1554.02	(0.07,16.54°)	1.12
	E	$\pi(d_{3/2}^{-2}s_{1/2}^{-2}h_{9/2}^{3})\otimes\nu[(fp)^4i_{13/2}^{-2}i_{11/2}^{1}]$	$\pi h_{9/2}^{1}\otimes\nu i_{11/2}^{1}$	−1551.56	(0.19,40.06°)	3.58
	F*	$\pi(d_{3/2}^{-2}s_{1/2}^{-2}h_{9/2}^{3})\otimes\nu[(fp)^4i_{13/2}^{-1}]$	$\pi h_{9/2}^{1}\otimes\nu i_{13/2}^{-1}$	−1555.44	(0.16,43.32°)	2.40
^{200}Tl	A	$\pi(s_{1/2}^{-2}h_{9/2}^{1})\otimes\nu[(fp)^6i_{13/2}^{-1}]$	$\pi h_{9/2}^{1}\otimes\nu i_{13/2}^{-1}$	−1570.57	(0.12,56.96°)	0
	B	$\pi(s_{1/2}^{-1})\otimes\nu[(fp)^5]$	$\pi s_{1/2}^{-1}\otimes\nu(fp)^1$	−1569.96	(0.02,1.92°)	0.61
	C	$\pi(d_{3/2}^{-1}s_{1/2}^{-2}h_{9/2}^{2})\otimes\nu[(fp)^6i_{13/2}^{-1}]$	$\pi d_{3/2}^{-1}\otimes\nu i_{13/2}^{-1}$	−1568.92	(0.14,53.48°)	1.65
	D	$\pi(d_{3/2}^{-1}s_{1/2}^{-2}h_{9/2}^{2})\otimes\nu[(fp)^6i_{13/2}^{-2}i_{11/2}^{1}]$	$\pi d_{3/2}^{-1}\otimes\nu i_{11/2}^{1}$	−1566.90	(0.17,48.94°)	3.67
	E	$\pi(d_{3/2}^{-2}s_{1/2}^{-2}h_{9/2}^{3})\otimes\nu[(fp)^6i_{13/2}^{-1}]$	$\pi h_{9/2}^{1}\otimes\nu i_{13/2}^{-1}$	−1566.80	(0.16,51.47°)	3.77
	F	$\pi(d_{3/2}^{-2}s_{1/2}^{-2}h_{9/2}^{3})\otimes\nu[(fp)^4i_{13/2}^{-1}i_{11/2}^{2}]$	$\pi h_{9/2}^{1}\otimes\nu i_{13/2}^{-1}$	−1564.53	(0.20,47.53°)	6.04

Table 2. Same as Table 1, but for the odd-mass nuclei $^{193-199}$Tl.

Nuclei	States	Configuration		$E_{\rm tot}$ /MeV	$(\beta,\gamma)^{\alpha}$	E_x(cal.) /MeV
		Valence nucleons	Unpaired nucleons			
^{193}Tl	A	$\pi(d_{3/2}^{-1}s_{1/2}^{-2}h_{9/2}^{2})\otimes\nu[(fp)^{2}i_{13/2}^{-4}]$	$\pi d_{3/2}^{-1}$	−1514.80	(0.18,38.38°)	0
	B	$\pi(s_{1/2}^{-2}h_{9/2}^{1})\otimes\nu[(fp)^{2}i_{13/2}^{-4}]$	$\pi h_{9/2}^{1}$	−1514.44	(0.15,37.06°)	0.36
	C	$\pi(d_{3/2}^{-2}s_{1/2}^{-2}h_{9/2}^{3})\otimes\nu[(fp)^{2}i_{13/2}^{-4}]$	$\pi h_{9/2}^{1}$	−1514.35	(0.20,35.54°)	0.45
	D	$\pi(s_{1/2}^{-1})\otimes\nu[(fp)^{2}i_{13/2}^{-4}]$	$\pi s_{1/2}^{-1}$	−1513.17	(0.10,0.21°)	1.63
	E	$\pi(s_{1/2}^{-1})\otimes\nu[i_{13/2}^{-2}]$	$\pi s_{1/2}^{-1}$	−1511.62	(0.05,0.36°)	3.18
	F*	$\pi(d_{3/2}^{-2}s_{1/2}^{-2}h_{9/2}^{3})\otimes\nu[f_{7/2}^{-2}(fp)^{4}i_{13/2}^{-4}]$	$\pi h_{9/2}^{1}\otimes\nu(i_{13/2}^{-1}i_{13/2}^{-1})$	−1514.27	(0.19,20.64°)	0.53
	G*	$\pi(d_{3/2}^{-2}s_{1/2}^{-2}h_{9/2}^{3})\otimes\nu[f_{7/2}^{-2}(fp)^{3}i_{13/2}^{-3}]$	$\pi h_{9/2}^{1}\otimes\nu[(fp)^{1}i_{13/2}^{-1}]$	−1514.13	(0.20,36.63°)	0.67
	H*	$\pi(s_{1/2}^{-2}h_{9/2}^{1})\otimes\nu[(fp)^{3}i_{13/2}^{-5}]$	$\pi h_{9/2}^{1}\otimes\nu[(fp)^{1}i_{13/2}^{-1}]$	−1513.94	(0.15,40.44°)	0.86
	I*	$\pi(d_{3/2}^{-2}s_{1/2}^{-2}h_{9/2}^{3})\otimes\nu[(fp)^{3}i_{13/2}^{-5}]$	$\pi h_{9/2}^{1}\otimes\nu[(fp)^{1}i_{13/2}^{-1}]$	−1513.36	(0.19,20.83°)	1.44
	J*	$\pi(s_{1/2}^{-2}h_{9/2}^{1})\otimes\nu[(fp)^{2}i_{13/2}^{-4}]$	$\pi h_{9/2}^{1}\otimes\nu(i_{13/2}^{-1}i_{13/2}^{-1})$	−1513.13	(0.14,39.64°)	1.67
^{195}Tl	A	$\pi(s_{1/2}^{-2}h_{9/2}^{1})\otimes\nu[(fp)^{4}i_{13/2}^{-4}]$	$\pi h_{9/2}^{1}$	−1531.52	(0.15,44.58°)	0
	B	$\pi(d_{3/2}^{-1}s_{1/2}^{-2}h_{9/2}^{2})\otimes\nu[(fp)^{4}i_{13/2}^{-4}]$	$\pi d_{3/2}^{-1}$	−1531.09	(0.18,40.86°)	0.43
	C	$\pi(d_{3/2}^{-2}s_{1/2}^{-2}h_{9/2}^{3})\otimes\nu[(fp)^{4}i_{13/2}^{-4}]$	$\pi h_{9/2}^{1}$	−1530.27	(0.20,38.38°)	1.25
	D	$\pi(s_{1/2}^{-1})\otimes\nu[(fp)^{4}i_{13/2}^{-4}]$	$\pi s_{1/2}^{-1}$	−1529.80	(0.11,25.12°)	1.73
	E	$\pi(s_{1/2}^{-1})$	$\pi s_{1/2}^{-1}$	−1528.19	(0.00,29.86°)	3.34
	F	$\pi(s_{1/2}^{-1})\otimes\nu[(fp)^{2}i_{13/2}^{-2}]$	$\pi s_{1/2}^{-1}$	–	–	–
	G	$\pi(s_{1/2}^{-2}h_{9/2}^{1})\otimes\nu[(fp)^{4}i_{13/2}^{-4}]$	$\pi h_{9/2}^{1}\otimes\nu(i_{13/2}^{-1}i_{13/2}^{-1})$	−1530.95	(0.15,46.12°)	0.57
	H	$\pi(s_{1/2}^{-2}h_{9/2}^{1})\otimes\nu[(fp)^{5}i_{13/2}^{-5}]$	$\pi h_{9/2}^{1}\otimes\nu[(fp)^{1}i_{13/2}^{-1}]$	−1530.92	(0.15,59.90°)	0.60
	I*	$\pi(s_{1/2}^{-2}h_{9/2}^{1})\otimes\nu[(fp)^{3}i_{13/2}^{-3}]$	$\pi h_{9/2}^{1}\otimes\nu[(fp)^{1}i_{13/2}^{-1}]$	−1530.73	(0.14,42.94°)	0.79
	J*	$\pi(d_{3/2}^{-2}s_{1/2}^{-2}h_{9/2}^{3})\otimes\nu[(fp)^{3}i_{13/2}^{-3}]$	$\pi h_{9/2}^{1}\otimes\nu[(fp)^{1}i_{13/2}^{-1}]$	−1529.96	(0.19,39.70°)	1.56
	K*	$\pi(d_{3/2}^{-2}s_{1/2}^{-2}h_{9/2}^{3})\otimes\nu[(fp)^{4}i_{13/2}^{-4}]$	$\pi h_{9/2}^{1}\otimes\nu(i_{13/2}^{-1}i_{13/2}^{-1})$	−1529.31	(0.19,43.75°)	2.21
	L	$\pi(d_{3/2}^{-2}s_{1/2}^{-2}h_{9/2}^{3})\otimes\nu[(fp)^{5}i_{13/2}^{-5}]$	$\pi h_{9/2}^{1}\otimes\nu[(fp)^{1}i_{13/2}^{-1}]$	−1527.74	(0.19,47.14°)	3.78
^{197}Tl	A	$\pi(s_{1/2}^{-2}h_{9/2}^{1})\otimes\nu[(fp)^{4}i_{13/2}^{-2}]$	$\pi h_{9/2}^{1}$	−1547.53	(0.13,35.83°)	0
	B	$\pi(d_{3/2}^{-1}s_{1/2}^{-2}h_{9/2}^{2})\otimes\nu[(fp)^{4}i_{13/2}^{-2}]$	$\pi d_{3/2}^{-1}$	−1547.10	(0.15,38.81°)	0.43
	C	$\pi(d_{3/2}^{-2}s_{1/2}^{-2}h_{9/2}^{3})\otimes\nu[(fp)^{4}i_{13/2}^{-2}]$	$\pi h_{9/2}^{1}$	−1546.01	(0.17,38.42°)	1.52
	D	$\pi(s_{1/2}^{-2}h_{9/2}^{1})\otimes\nu[(fp)^{2}]$	$\pi s_{1/2}^{-1}$	−1545.57	(0.09,47.61°)	1.96
	E	$\pi(s_{1/2}^{-1})\otimes\nu[(fp)^{2}]$	$\pi s_{1/2}^{-1}$	−1544.92	(0.04,59.83°)	2.61
	F*	$\pi(s_{1/2}^{-2}h_{9/2}^{1})\otimes\nu[(fp)^{5}i_{13/2}^{-3}]$	$\pi h_{9/2}^{1}\otimes\nu[(fp)^{1}i_{13/2}^{-1}]$	−1546.73	(0.13,43.18°)	0.8
	G*	$\pi(s_{1/2}^{-2}h_{9/2}^{1})\otimes\nu[(fp)^{4}i_{13/2}^{-2}]$	$\pi h_{9/2}^{1}\otimes\nu(i_{13/2}^{-1}i_{13/2}^{-1})$	−1546.38	(0.12,40.51°)	1.15
	H*	$\pi(s_{1/2}^{-2}h_{9/2}^{1})\otimes\nu[(fp)^{3}i_{13/2}^{-1}]$	$\pi h_{9/2}^{1}\otimes\nu[(fp)^{1}i_{13/2}^{-1}]$	−1546.17	(0.12,41.97°)	1.36
	I*	$\pi(d_{3/2}^{-2}s_{1/2}^{-2}h_{9/2}^{3})\otimes\nu[(fp)^{3}i_{13/2}^{-1}]$	$\pi h_{9/2}^{1}\otimes\nu[(fp)^{1}i_{13/2}^{-1}]$	−1544.54	(0.17,43.72°)	2.99
	J*	$\pi(s_{1/2}^{-2}i_{13/2}^{1})\otimes\nu[(fp)^{3}i_{13/2}^{-1}]$	$\pi i_{13/2}^{1}\otimes\nu[(fp)^{1}i_{13/2}^{-1}]$	−1542.89	(0.12,43,29°)	4.64
^{199}Tl	A	$\pi(s_{1/2}^{-2}h_{9/2}^{1})\otimes\nu[(fp)^{6}i_{13/2}^{-2}]$	$\pi h_{9/2}^{1}$	−1562.83	(0.13,50.63°)	0
	B	$\pi(s_{1/2}^{-2}h_{9/2}^{1})\otimes\nu[(fp)^{4}]$	$\pi h_{9/2}^{1}$	−1562.09	(0.11,53.31°)	0.74
	C	$\pi(s_{1/2}^{-1})\otimes\nu[(fp)^{4}]$	$\pi s_{1/2}^{-1}$	−1561.87	(0.03,0.73°)	0.96
	D	$\pi(d_{3/2}^{-1}s_{1/2}^{-2}h_{9/2}^{2})\otimes\nu[(fp)^{6}i_{13/2}^{-2}]$	$\pi d_{3/2}^{-1}$	−1561.34	(0.15,48.46°)	1.49
	E	$\pi(s_{1/2}^{-2}h_{9/2}^{1})\otimes\nu[(fp)^{6}i_{13/1}^{-2}]$	$\pi h_{9/2}^{1}\otimes\nu(i_{13/2}^{-1}i_{13/2}^{-1})$	−1562.51	(0.13,59.96°)	0.32
	F	$\pi(s_{1/2}^{-2}h_{9/2}^{1})\otimes\nu[(fp)^{5}i_{13/2}^{-1}]$	$\pi h_{9/2}^{1}\otimes\nu[(fp)^{1}i_{13/2}^{-1}]$	−1562.31	(0.12,51.80°)	0.52
	G	$\pi(s_{1/2}^{-2}h_{9/2}^{1})\otimes\nu[(fp)^{7}i_{13/2}^{-3}]$	$\pi h_{9/2}^{1}\otimes\nu[(fp)^{1}i_{13/2}^{-1}]$	−1561.58	(0.13,51.24°)	1.25

Figures and Tables. In what follows, the possible candidate states of chirality and MχD in thallium isotopes are discussed for odd-odd and odd-mass nuclei, respectively.

A. Candidate chiral nuclei in odd-odd thallium isotopes

For ^{192}Tl, as shown in Table 1, the states D* and H* with the proper particle-hole configuration $\pi h^{1}_{9/2}\otimes\nu i^{-1}_{13/2}$ and triaxial deformation ($\beta=0.21$, $\gamma=39.84^\circ$ and $\beta=0.16$, $\gamma=26.17^\circ$) are suitable to form the chiral doublet bands. Thus, two sets of chiral doublet bands based on the states D* and H*, namely the MχD bands, are expected in ^{192}Tl.

A type of MχD bands, namely four bands with identical configuration, have been reported experimentally in ^{103}Rh [93]. Here, the mechanism of the possible MχD bands in ^{192}Tl is different from that of the four bands in ^{103}Rh. It is worth noting that the states D* and H* have the same unpaired nucleon configuration $\pi h^{1}_{9/2}\otimes\nu i^{-1}_{13/2}$ but exhibit some differences in the triaxial deformation and valence nucleon configuration (D*: $\pi(d^{-2}_{3/2}s^{-2}_{1/2}h^{3}_{9/2})\otimes\nu[(fp)^2 i^{-5}_{13/2}]$, H*: $\pi(s^{-2}_{1/2}h^{1}_{9/2})\otimes\nu(i^{-3}_{13/2})$). This type of MχD in ^{192}Tl is interesting to explore experimentally.

For ^{194}Tl, as shown in Table 1, the states C* ($\beta=0.14,\gamma=36.81^\circ$) and H* ($\beta=0.17,\gamma=18.80^\circ$), related to the same unpaired nucleon configuration $\pi h^{1}_{9/2}\otimes\nu i^{-1}_{13/2}$, are obtained in the calculations. The present calculations support the existence of chiral doublet bands in ^{194}Tl, and there is a possibility to form the MχD. Ref. [61] suggested that two negative bands form an excellent candidate for chiral doublet bands built on the $\pi h^{1}_{9/2}\otimes\nu i^{-1}_{13/2}$ configuration below the band crossing and the $\pi h^{1}_{9/2}\otimes\nu i^{-3}_{13/2}$ configuration above the band crossing. To compare with the experimental results above the band crossing, we further perform the particle-hole excitation to the four-quasiparticle configuration. State I* with the triaxial deformation ($\beta=0.13,\gamma=45.19^\circ$) and $\pi h^{1}_{9/2}\otimes\nu i^{-3}_{13/2}$ configuration is obtained in the calculations, which is conducive to the formation of chirality.

For ^{196}Tl, as shown in Table 1, the states A* ($\beta=0.13,\gamma=34.88^\circ$), E*($\beta=0.18,\gamma=37.26^\circ$), and H*($\beta=0.12,\gamma=42.75^\circ$) have the same unpaired nucleon configuration $\pi h^{1}_{9/2}\otimes\nu i^{-1}_{13/2}$. Compared with ^{192,194}Tl, the hole-like nature of the valence neutron in ^{196}Tl is better, which might be more suitable for the appearance of the chiral doublet bands. Theoretical calculations suggest the MχD in ^{196}Tl combined by six $\Delta I=1$ bands based on the $\pi h^{1}_{9/2}\otimes\nu i^{-1}_{13/2}$ configuration.

For ^{198}Tl, as shown in Table 1, the states B* ($\beta=0.11,\gamma=39.43^\circ$) and F* ($\beta=0.16,\gamma=43.32^\circ$), related to the same unpaired nucleon configuration $\pi h^{1}_{9/2}\otimes\nu i^{-1}_{13/2}$, are obtained in the calculations. The present calculations support the existence of chiral doublet bands in ^{198}Tl, and the phenomenon of MχD is also highly expected. Similar to ^{194}Tl, chiral doublet bands based on the $\pi h^{1}_{9/2}\otimes\nu i^{-1}_{13/2}$ configuration have also been observed experimentally in ^{198}Tl [64, 65], and the two-quasiparticle-plus-triaxial-rotor model calculations show excellent agreement with the experimental data for $\gamma=44^\circ$ [65], which is in good agreement with our results.

Based on the above discussion for odd-odd thallium isotopes, the calculations suggest the existence of chiral doublet bands based on the configuration $\pi h^{1}_{9/2}\otimes\nu i^{-1}_{13/2}$ in ^{192,194,196,198}Tl, as well as the configuration $\pi h^{1}_{9/2}\otimes\nu i^{-1}_{13/2}i^{-1}_{13/2}i^{-1}_{13/2}$ in ^{194}Tl. In experiments, the chiral doublet bands in ^{194,198}Tl with the configuration $\pi h^{1}_{9/2}\otimes\nu i^{-1}_{13/2}$ have been reported [61, 64, 65], and a rotational band with the same configuration was observed in ^{192}Tl [94, 95] and ^{196}Tl [96], respectively. To study the systematic properties of these rotational bands, the excitation energies and transition probability ratios $B(M1)/B(E2)$ of the main band and its chiral partner band (if it exists) with the $\pi h^{1}_{9/2}\otimes\nu i^{-1}_{13/2}$ configuration in ^{192,194,196,198}Tl are plotted in Fig. 4 (a-h). As shown in Fig. 4 (a-h), the energy spectra and $B(M1)/B(E2)$ values of the negative-parity band in ^{192,196}Tl are in accordance with the systematics of the adjacent odd-odd chiral nuclei ^{194,198}Tl, which also implies the existence of chirality in ^{192,196}Tl. Furthermore, MχD bands based on the same unpaired nucleon configuration $\pi h^{1}_{9/2}\otimes\nu i^{-1}_{13/2}$ but different triaxial deformation and nucleon occupation are predicted in ^{192,194,196,198}Tl. It would be interesting to explore these MχD bands experimentally.

B. Candidate chiral nuclei in odd-mass thallium isotopes

For the odd-mass thallium isotopes, the calculation of the adiabatic and configuration-fixed constrained triaxial RMF is similar to that for the odd-odd nucleus, except for performing the particle-hole excitation to three-quasiparticle configurations. Two types of three-quasiparticle chiral configurations can be expected for the odd-mass thallium isotopes: one occurs when a low-j-shell neutron (which acts as a spectator) is coupled to the neighboring odd-odd chiral configuration; the second is formed by an aligned pair of high-j $i_{13/2}$ neutron holes, i.e., $\pi h^{1}_{9/2}\otimes\nu i^{-1}_{13/2}i^{-1}_{13/2}$.

For ^{193}Tl, as shown in Table 2, states B ($\beta=0.15$, $\gamma=37.06^\circ$) and C ($\beta=0.20,\gamma=35.54^\circ$) have the triaxial deformation and the same unpaired nucleon configuration $\pi h^{1}_{9/2}$. We perform the excitation based on states B and C to obtain the states F*, G*, H*, I*, J*, which have prominent triaxial deformation. The configurations are $\pi h^{1}_{9/2}\otimes\nu i^{-1}_{13/2}i^{-1}_{13/2}$ for states F*, J* and $\pi h^{1}_{9/2}\otimes\nu(fp)^1 i^{-1}_{13/2}$ for states G*, H*, I*, which are suitable for the appear-

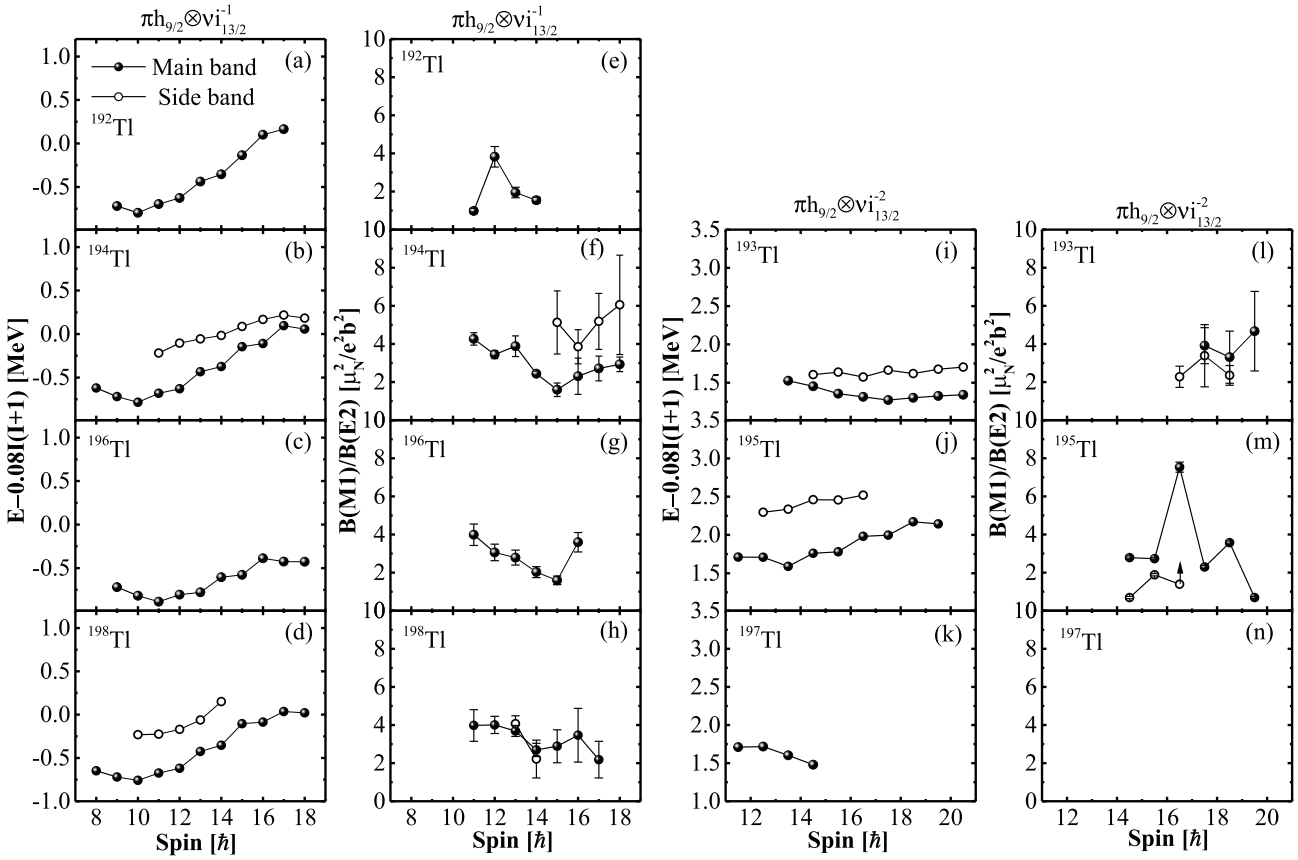

Fig. 4. Excitation energies and $B(M1)/B(E2)$ values of the main band and its chiral partner (if it exists) with the $\pi h^1_{9/2}\otimes\nu i^{-1}_{13/2}$ configuration in ^{192,194,196,198}Tl (a-h) and the $\pi h^1_{9/2}\otimes\nu(i^{-1}_{13/2}i^{-1}_{13/2})$ configuration in ^{193,195,197}Tl (i-n). The experimental data have been obtained from Refs. [24, 60, 61, 64, 65, 94–98].

ance of chirality. Thus, MχD combined by three sets of positive-parity chiral doublet bands and two sets of negative-parity chiral doublet bands are expected to be observed in ^{193}Tl according to the calculations.

For ^{195}Tl, similar to ^{193}Tl, states I*, J* with configuration $\pi h^1_{9/2}\otimes\nu(fp)^1 i^{-1}_{13/2}$, and state K* with configuration $\pi h^1_{9/2}\otimes\nu i^{-1}_{13/2}i^{-1}_{13/2}$ are obtained with prominent triaxial deformation, which can possibly form the chiral doublet bands. Thus, MχD with three-quasiparticle configurations combined by two sets of positive-parity chiral doublet bands and one set of negative-parity chiral doublet bands are expected to be observed in ^{195}Tl according to the calculations. Prior to this work, RMF calculations for ^{195}Tl were also performed in Ref. [50]. The deformations and excitation energies for the low lying states A ($\pi h^1_{9/2}$), D ($\pi s^{-1}_{1/2}$), and G [$\pi h^1_{9/2}\otimes\nu(i^{-1}_{13/2}i^{-1}_{13/2})$] (corresponding to the A, B, and C states in Ref. [50]) are consistent with the calculated results in Ref. [50]. The present calculation cannot provide the five-quasiparticle states. In addition, chiral doublet bands based on states I*, J* have never been reported experimentally in the nucleus, which is worth exploring further.

For ^{197}Tl, similar to ^{193,195}Tl, states F*, H*, I* with configuration $\pi h^1_{9/2}\otimes\nu(fp)^1 i^{-1}_{13/2}$, state G* with configuration $\pi h^1_{9/2}\otimes\nu i^{-1}_{13/2}i^{-1}_{13/2}$, and state J* with configuration $\pi i^1_{13/2}\otimes\nu(fp)^1 i^{-1}_{13/2}$ are obtained with prominent triaxial deformation, which can possibly form the chiral doublet bands. Thus, MχD with three-quasiparticle configurations combined by three sets of positive-parity chiral doublet bands and two sets of negative-parity chiral doublet bands are expected to be observed in ^{197}Tl according to the calculations. In addition, a pair of negative-parity rotational bands (B2 and B3 bands in Ref. [97]) were found with the assigned configuration $\pi i^1_{13/2}\otimes\nu(fp)^1 i^{-1}_{13/2}$ in ^{197}Tl, and whether or not chirality exists in these two bands remains an open question.

Based on the above discussion for odd-mass thallium isotopes, the calculations suggest the possible formations of chirality based on the configurations $\pi h^1_{9/2}\otimes\nu i^{-1}_{13/2}i^{-1}_{13/2}$ and $\pi h^1_{9/2}\otimes\nu(fp)^1 i^{-1}_{13/2}$ in ^{193,195,197}Tl, as well as the configuration $\pi i^1_{13/2}\otimes\nu(fp)^1 i^{-1}_{13/2}$ in ^{197} Tl. Compared with the calculated results for the odd-odd thallium isotopes, there are more candidate states to form chirality obtained in odd-mass isotopes. In experiments, candidate chiral doublet bands with the configuration $\pi h^1_{9/2}\otimes\nu i^{-1}_{13/2}i^{-1}_{13/2}$

have been reported in ^{193}Tl [60] and ^{195}Tl [24]. A rotational band based on the same configuration in ^{197}Tl has been observed [97]. The excitation energies and $B(M1)/B(E2)$ values of these observed bands are shown in Fig. 4 (i-n). As shown in Fig. 4 (i-n), the energy spectrum of the band in ^{197}Tl is in accordance with the systematics of the adjacent odd-A chiral nuclei ^{193,195}Tl, but the corresponding $B(M1)/B(E2)$ values are still lacking. Therefore, further experiments are necessary to study the band in ^{197}Tl and search for its chiral partner. Furthermore, the phenomenon of MχD bands based on the above configurations in ^{193,195,197}Tl should be explored experimentally.

IV. SUMMARY

The chirality in thallium isotopes was investigated using the adiabatic and configuration-fixed constrained triaxial relativistic mean field theory. The calculations suggest that the configuration $\pi h^1_{9/2}\otimes\nu i^{-1}_{13/2}$ in odd-odd nuclei ^{192,194,196,198}Tl, configuration $\pi h^1_{9/2}\otimes\nu i^{-1}_{13/2}i^{-1}_{13/2}i^{-1}_{13/2}$ in ^{194}Tl, configurations $\pi h^1_{9/2}\otimes\nu i^{-1}_{13/2}i^{-1}_{13/2}$ & $\pi h^1_{9/2}\otimes\nu(fp)^1 i^{-1}_{13/2}$ in odd-mass nuclei ^{193,195,197}Tl, and configuration $\pi i^1_{13/2}\otimes\nu(fp)^1 i^{-1}_{13/2}$ in ^{197}Tl with their triaxial deformations favor the existence of chirality. As the chiral doublet bands in ^{193,194,195,198}Tl have been reported, the chiral doublet bands in ^{192,196,197}Tl are expected to be observed experimentally.

Furthermore, the possible existence of MχD bands is demonstrated in ^{192,193,194,195,196,197,198}Tl. MχD bands based on the same unpaired nucleon configuration but different triaxial deformation and nucleon occupation are predicted. It would be interesting to explore the phenomenon of MχD bands in thallium isotopes experimentally.

This paper will motivate an experimental investigation of these nuclei with the possibility to confirm the predicted chirality and MχD in thallium isotopes and facilitate the search for a possible "island of chiral nuclei" in the 190 mass region.

References

[1] S. Frauendorf and J. Meng, Nucl. Phys. A **617**, 131 (1997)
[2] K. Starosta *et al*., Phys. Rev. Lett. **86**, 971 (2001)
[3] S. Frauendorf, Rev. Mod. Phys. **73**, 463 (2001)
[4] J. Meng and S. Q. Zhang, J. Phys. G: Nucl. Part. Phys. **37**, 064025 (2010)
[5] J. Meng, Q. B. Chen, and S. Q. Zhang, Int. J. Mod. Phys. E **23**, 1430016 (2013)
[6] B. W. Xiong and Y. Y.Wang, At. Data Nucl. Data Tables **125**, 193 (2019)
[7] S. Y. Wang, Chin. Phys. C **44**, 11 (2020)
[8] X. C. Han *et al*., Phys. Rev. C **104**, 014327 (2021)
[9] L. Mu *et al*., Phys. Lett. B **827**, 137006 (2022)
[10] W. Z. Xu *et al*., (in preparation)
[11] X. Xiao *et al*., (in preparation)
[12] J. Meng *et al*., Phys. Rev. C **73**, 037303 (2006)
[13] C. Liu *et al*., Phys. Rev. Lett. **116**, 112501 (2016)
[14] I. Kuti *et al*., Phys. Rev. Lett. **113**, 032501 (2014)
[15] J. Timár *et al*., Phys. Lett. B **598**, 178 (2004)
[16] J. A. Alcántara-Núñez *et al*., Phys. Rev. C **69**, 024317 (2004)
[17] D. Jerrestam *et al*., Nucl. Phys. A **577**, 786 (1994)
[18] F. R. Espinoza-Quiñones *et al*., Phys. Rev. C **55**, 1548 (1997)
[19] B. Zhang *et al*., Chin. Phys. C **35**, 1009 (2011)
[20] A. D. Ayangeakaa *et al*., Phys. Rev. Lett. **110**, 172504 (2013)
[21] S. Zhu *et al*., Phys. Rev. Lett. **91**, 132501 (2003)
[22] B. F. Lv *et al*., Phys. Rev. C **100**, 024314 (2019)
[23] C. M. Petrache *et al*., Phys. Rev. C **97**, 041304(R) (2018)
[24] T. Roy *et al*., Phys. Lett. B **782**, 768 (2018)
[25] V. I. Dimitrov, S. Frauendorf, and F. Dönau, Phys. Rev. Lett. **84**, 5732 (2000)
[26] P. Olbratowski *et al*., Phys. Rev. Lett. **93**, 052501 (2004)
[27] P. W. Zhao, S. Q. Zhang, and J. Meng, Phys. Rev. C **92**, 034319 (2015)
[28] P. W. Zhao, Phys. Lett. B **773**, 1 (2017)
[29] Z. X. Ren, P. W. Zhao, and J. Meng, Phys. Rev. C **105**, L011301 (2022)
[30] J. Peng, J. Meng, and S. Q. Zhang, Phys. Rev. C **68**, 044324 (2003)
[31] T. Koike, K. Starosta, and I. Hamamoto, Phys. Rev. Lett. **93**, 172502 (2004)
[32] S. Y. Wang *et al*., Phys. Rev. C **75**, 024309 (2007)
[33] S. Q. Zhang *et al*., Phys. Rev. C **75**, 044307 (2007)
[34] S. Y. Wang *et al*., Phys. Rev. C **77**, 034314 (2008)
[35] J. Meng *et al*., Mod. Phys. Lett. A **23**, 2560 (2008)
[36] B. Qi *et al*., Phys. Lett. B **675**, 175 (2009)
[37] B. Qi *et al*., Phys. Rev. C **79**, 041302 (2009)
[38] S. Y. Wang, B. Qi, and D. P. Sun, Phys. Rev. C **82**, 027303 (2010)
[39] Q. B. Chen *et al*., Phys. Rev. C **82**, 067302 (2010)
[40] E. A. Lawrie and O. Shirinda, Phys. Lett. B **689**, 66 (2010)
[41] B. Qi, S. Q. Zhang, and S. Y. Wang, Phys. Rev. C **83**, 034303 (2011)
[42] O. Shirinda and E. A. Lawrie, Eur. Phys. J. A **48**, 118 (2012)
[43] I. Hamamoto, Phys. Rev. C **88**, 024327 (2013)
[44] H. Jia *et al*., Chin. Phys. C **40**, 124103 (2016)
[45] Q. B. Chen *et al*., Phys. Lett. B **782**, 744 (2018)
[46] Y. Y. Wang *et al*., Phys. Lett. B **792**, 454 (2019)
[47] J. Peng and Q. B. Chen, Phys. Lett. B **793**, 303 (2019)
[48] Y. P. Wang *et al*., Phys. Rev. C **102**, 024313 (2020)
[49] Q. B. Chen *et al*., Phys. Lett. B **807**, 135568 (2020)
[50] J. Peng and Q. B. Chen, Phys. Lett. B **806**, 135489 (2020)
[51] S. Brant and C. M. Petrache, Phys. Rev. C **79**, 054326 (2009)
[52] H. G. Ganev and S. Brant, Phys. Rev. C **82**, 034328 (2010)
[53] Q. B. Chen *et al*., Phys. Rev. C **87**, 024314 (2013)
[54] Q. B. Chen *et al*., Phys. Rev. C **94**, 044301 (2016)
[55] F. Q. Chen *et al*., Phys. Rev. C **96**, 051303 (2017)
[56] F. Q. Chen, J. Meng, and S. Q. Zhang, Phys. Lett. B **785**, 211 (2018)

[57] S. Mukhopadhyay *et al*., Phys. Rev. Lett. **99**, 172501 (2007)
[58] Y. Zhang, B. Qi, and S. Q. Zhang, Sci. China-Phys. Mech. Astron. **64**, 122011 (2021)
[59] J. Ndayishimye *et al*., Acta Physica Polonica B **48**, 343 (2017)
[60] J. Ndayishimye *et al*., Phys. Rev. C **100**, 014313 (2019)
[61] P. L. Masiteng *et al*., Eur. Phys. J. A. **50**, 119 (2014)
[62] P. L. Masiteng *et al*., AIP Conference Proceedings **1377**, 392 (2011)
[63] P. L. Masiteng *et al*., Phys. Lett. B **719**, 83 (2013)
[64] E. A. Lawrie *et al*., Phys. Rev. C **78**, 021305 (2008)
[65] E. A. Lawrie *et al*., Eur. Phys. J. A. **45**, 39 (2010)
[66] D. L. Balabanski *et al*., Phys. Rev. C **70**, 044305 (2004)
[67] J. Meng, *Relativistic Density Functional for Nuclear Structure* (World Scientific, Singapore, 2015)
[68] D. Vretenar *et al*., Phys. Rep. **409**, 101 (2005)
[69] J. Meng *et al*., Prog. Part. Nucl. Phys. **57**, 470 (2006)
[70] J. Meng *et al*., J. Phys. G **42**, 093101 (2015)
[71] J. Meng *et al*., Phys. Rev. C **58**, 628 (1998)
[72] T. S. Chen *et al*., Chin. Phys. Lett. **20**, 358 (2003)
[73] S. G. Zhou, J. Meng, and P. Ring, Phys. Rev. Lett. **91**, 262501 (2003)
[74] H. Z. Liang, J. Meng, and S. G. Zhou, Phys. Rep. **570**, 1 (2015)
[75] J. Meng *et al*., Phys. Rev. C **59**, 159 (1999)
[76] H. Z. Liang, N. V. Giai, and J. Meng, Phys. Rev. Lett. **101**, 122502 (2008)
[77] J. Meng and P. W. Zhao, Phys. Scr. **91**, 053008 (2016)
[78] P. W. Zhao *et al*., Phys. Rev. C **82**, 054319 (2010)
[79] H. Jia *et al*., Phys. Rev. C **97**, 024335 (2018)
[80] J. Peng and Q. B. Chen, Phys. Rev. C **98**, 024320 (2018)
[81] C. Liu *et al*., Chin. Phys. Lett. **37**, 112101 (2020)
[82] B. Qi *et al*., Sci. China-Phys. Mech. Astron. **62**, 012012 (2019)
[83] B. Qi *et al*., Phys. Rev. C **98**, 014305 (2018)
[84] J. Peng *et al*., Phys. Rev. C **77**, 024309 (2008)
[85] J. M. Yao *et al*., Phys. Rev. C **79**, 067302 (2009)
[86] J. Li and S. Q. Zhang, Phys. Rev. C **83**, 037301 (2011)
[87] B. Qi *et al*., Phys. Rev. C **88**, 027302 (2013)
[88] J. Li, Phys. Rev. C **97**, 034306 (2018)
[89] W. H. Long *et al*., Phys. Rev. C **69**, 034319 (2004)
[90] G. A. Lalazissis, J. König, and P. Ring, Phys. Rev. C **55**, 540 (1997)
[91] C. B. Li *et al*., Phys. Rev. C **97**, 034331 (2018)
[92] S. Bhattacharya *et al*., Phys. Rev. C **95**, 014301 (2017)
[93] J. Timár *et al*., Phys. Rev. C **73**, 011301 (2006)
[94] A. J. Kreiner *et al*., Phys. Rev. C **21**, 993 (1980)
[95] L. L. Riedinger *et al*., No. ANL–PHY/CP, 89541 (1996)
[96] A. J. Kreiner, M. Fenzl, and W. Kutschera, Nucl. Phys. A **308**, 147 (1978)
[97] H. Pai *et al*., Phys. Rev. C **88**, 064302 (2013)
[98] Evaluated Nuclear Structure Data File Retrieval, http://www.nndc.bnl.gov/ensdf/.